Ultrastructural Organization of Amyloid Fibrils by Atomic Force Microscopy

Aaron K. Chamberlain ,* Cait E. MacPhee,* Jesús Zurdo,* Ludmilla A. Morozova-Roche,* H. Allen O. Hill,† Christopher M. Dobson,* and Jason J. Davis†

*Oxford Centre for Molecular Sciences, New Chemistry Laboratory, and †Inorganic Chemistry Laboratory, University of Oxford, Oxford OX1 3QT, United Kingdom

ABSTRACT Atomic force microscopy has been employed to investigate the structural organization of amyloid fibrils produced in vitro from three very different polypeptide sequences. The systems investigated are a 10-residue peptide derived from the sequence of transthyretin, the 90-residue SH3 domain of bovine phosphatidylinositol-3′-kinase, and human wild-type lysozyme, a 130-residue protein containing four disulfide bridges. The results demonstrate distinct similarities between the structures formed by the different classes of fibrils despite the contrasting nature of the polypeptide species involved. SH3 and lysozyme fibrils consist typically of four protofilaments, exhibiting a left-handed twist along the fibril axis. The substructure of TTR_{10-19} fibrils is not resolved by atomic force microscopy and their uniform appearance is suggestive of a regular self-association of very thin filaments. We propose that the exact number and orientation of protofilaments within amyloid fibrils is dictated by packing of the regions of the polypeptide chains that are not directly involved in formation of the cross-β core of the fibrils. The results obtained for these proteins, none of which is directly associated with any human disease, are closely similar to those of disease-related amyloid fibrils, supporting the concept that amyloid is a generic structure of polypeptide chains. The detailed architecture of an individual fibril, however, depends on the manner in which the protofilaments assemble into the fibrillar structure, which in turn is dependent on the sequence of the polypeptide and the conditions under which the fibril is formed.

INTRODUCTION

A range of debilitating human diseases is associated with the conversion of proteins, or fragments of proteins, from their normally soluble forms into insoluble fibrils or plaques, which accumulate in a variety of organs (Kelly, 1998; Lansbury, 1999; Perutz, 1999). The insoluble material, known as amyloid, has a well-defined fibrillar structure. The diseases associated with amyloid can be sporadic, inherited, or even infectious, and the protein aggregates are thought to be the direct or indirect origin of the disease in question. These include Alzheimer's and Parkinson's diseases, the spongiform encephalopathies such as Creutzfeldt-Jakob disease, and adult-onset (type II) diabetes (Serpell et al., 1997; Koo et al., 1999). Remarkably, despite the range of proteins involved in these diseases, all of which have unique and characteristic native folds, the fibrils in which they are found in the disease states have structurally similar characteristics (Sunde et al., 1997). Striking evidence has recently accumulated suggesting that the ability to form amyloid is not a peculiarity of this small group of disease-related proteins (Guijarro et al., 1998b; Chiti et al., 1999) but, rather, that the ability to form amyloid is a generic property of the polypeptide chain. The phenomenon can be explained by the fact that the intermolecular bonds that stabilize this material involve the peptide backbone, which is common to all proteins (Dobson, 1999).

Three-dimensional models have been generated to describe the assembly of fibrils by a number of proteins, including the disease-related protein human plasma protein transthyretin (Serpell et al., 1995; Blake et al., 1996; Blake and Serpell, 1996), the Aβ peptide implicated in Alzheimer's disease (Fraser et al., 1991; Chaney et al., 1998; Malinchik et al., 1998; Li et al., 1999; Tjernberg et al., 1999), and a src homology (SH3) domain that has no known role in any disease (Jiménez et al., 1999). The model of the transthyretin filament consists of four protofilaments that are associated to form a twisted fibril. Each protofilament consists of four β-sheets packed together with a separation of $\sim$1 nm, which twists along its long axis every 11.5 nm or approximately every 24 β-strands, resulting in a protofilament diameter of 5–6 nm (Blake and Serpell, 1996). The models suggested to explain the structure of Aβ peptide fibrils implicate pairs of β-sheets assembling to form a protofilament $>$2 nm in diameter, three to five of which associate in the formation of the fibril. Solid-state nuclear magnetic resonance (NMR) has been employed to probe the orientation of the strands in the β-sheet core of fibrils formed by fragments of the Aβ peptide. Whereas $A\beta_{34-42}$ adopts an anti-parallel orientation in the assembled fibrils (Lansbury et al., 1995), the peptide $A\beta_{10-35}$ is found in a parallel alignment of β-sheets (Benzinger et al., 1998) implying that the details of the protofilament structure may be critically dependent on the exact peptide sequence and the

Received for publication 9 February 2000 and in final form 29 August 2000.

A.K.C., C.E.M., J.Z., and L.A.M.-R. contributed equally to this work.

Address reprint requests to Dr. Jason J. Davis, Inorganic Chemistry Laboratory, University of Oxford, South Parks Road, Oxford OX1 3QR, UK. Tel.: 44-0-1865-275900; Fax: 44-1865-272690; E-mail: jason.davis@chem.ox.ac.uk.

0006-3495/00/12/3282/12 $2.00

conditions under which the fibril forms. Only by examining the structures of a range of different amyloid fibrils will we obtain a full understanding of the relationship between their structure and formation. In the work described in this paper, we have employed atomic force microscopy (AFM) to study the ultrastructure of amyloid fibrils assembled from three very different protein precursors.

AFM is now a significant contributor to the field of structural biology (Shao and Yang, 1995; Shao et al., 1995; Shao and Zhang, 1996) and several reviews have accordingly been published recently (Shao et al., 1995; Engel et al., 1999; Heinz and Hoh, 1999). The power of this method lies in the high-resolution three-dimensional structural detail attainable without the need to average over a number of objects, combined with the ability to image samples under controlled fluid conditions. Delicate biological specimens can thus be spared the harsh treatments often employed in electron microscopy (e.g., fixation or staining) or x-ray fiber diffraction. The imaging of protein-based samples is not, however, straightforward. The mechanical instability associated with AFM operation in the contact mode sets a lower limit for the imaging force that can be used, and the high lateral loading force imparted by the scanning AFM tip commonly leads to sample distortion, sweeping, and/or gross image distortion. By using a tapping mode, in which the scanning probe is oscillated sinusoidally and gently taps the sample of interest, reproducible images of high quality can be obtained. In this mode of operation, individual biomolecules can be investigated in air or in solution (Hansma and Hoh, 1994).

The three types of fibrils chosen for investigation represent extremes of precursor proteins that self-assemble into amyloid. The first is composed of the 10-residue peptide TTR_{10-19}, derived from the sequence of the human plasma protein transthyretin. This peptide, corresponding to an isolated β-strand in the native structure of TTR, has previously been shown to assemble readily into amyloid fibrils in vitro (Gustavsson et al., 1991) exhibiting a typical cross-β conformation in x-ray diffraction studies (Jarvis et al., 1993). The second type of fibril is assembled from the 90-residue, predominantly β-sheet, SH3 domain of bovine phosphatidylinositol-3′-kinase (PI-3′-kinase; Guijarro et al., 1998b). A high-resolution structural model of these fibrils has been constructed from cryoelectron microscopy data (Jiménez et al., 1999). The third type is assembled from the 130-residue wild-type sequence of the human protein lysozyme. The native structure of lysozyme contains both α-helical and β-sheet domains, including four disulfide bonds. Lysozyme has recently become the focus of intensive research due to the isolation and characterization of two naturally occurring mutants that give rise to a hereditary amyloidosis in humans (Pepys et al., 1993; Booth et al., 1997; Canet et al., 1999), and the recent finding that the well-characterized wild-type protein also assembles to form fibrils (Morozova-Roche et al., 2000).

MATERIALS AND METHODS

Fibril preparation

TTR_{10-19}

TTR_{10-19} (CPLMVKVLDA) was synthesized on an Applied Biosystems 430A automated peptide synthesizer using standard Fmoc chemistry. After cleavage from the support, the peptide was purified by reverse-phase high-performance liquid chromatography (RP-HPLC) on a Beckman System Gold HPLC using either an analytical Brownlee 4.6 × 30 mm C8 reverse-phase column or a preparative Vydac 10 × 250 mm C-18 reverse phase column. Fractions eluting from the column were analyzed by mass spectrometry, and those of the desired molecular weight were pooled and lyophilized.

Amyloid fibrils were formed by dissolution of TTR_{10-19} at 10 mg/ml in 10% (v/v) CH_3COOH, pH 2, followed by incubation for 7–14 days at room temperature. Fibril formation was assessed by transmission electron microscopy and by the observation of β-sheet secondary structure by circular dichroism spectroscopy. The reducing agent dithiothreitol (DTT) was added to fibril preparations to determine whether elimination of disulfide bonds influenced the morphology of fibrils formed in acidic solution. The results indicate that reduction of the cysteine residue at position 1 in the peptide sequence does not detectably influence the fibril ultrastructure as assessed by electron microscopy (EM). Typically, the percentage of peptide present as disulfide-linked dimers in peptide preparations was ~20%, as determined by MALDI-TOF mass spectrometry.

SH3 domain

The recombinant SH3 domain used in this study consists of 84 residues derived from the p85α subunit of bovine PI-3′-kinase plus a two-residue (Gly-Ser) N-terminal extension and a four-residue (Trp-Asn-Ser-Ser) C-terminal extension. The expression and purification procedures used here have been described previously (Booker et al., 1993; Guijarro et al., 1998a). Briefly, the polypeptide was expressed in *Escherichia coli* strain BL21 as a fusion to glutathione S transferase. After induction with isopropyl-β-D-thiogalactopyranoside, the fusion protein was purified over a GST-Sepharose column, cleaved with thrombin, and further purified through Mono Q ion exchange and S-100 size exclusion columns. The purified protein was dialyzed into 20 mM ammonium bicarbonate and lyophilized. Fibrils were generated by dissolving the protein to 0.5 mM in D_2O adjusted to pH 2.0 (isotope corrected) with DCl and allowing prolonged (>2 weeks) incubation at 35°C. Fourier transform infrared spectroscopy and EM were employed to assess fibril formation.

Metal shadowing of SH3 amyloid fibrils

Samples containing SH3 domain amyloid fibrils (prepared as indicated above) were diluted 50-fold and sprayed onto a freshly cleaved mica sheet. The sheets were vacuum dried before platinum shadowing was carried out by melting a small portion of platinum wire onto a carbon rod and evaporating the metal onto the sample using a conventional carbon coater (positioning the mica sheets at an angle of 15° to the surface). The plates were then placed flat and coated with carbon. Samples were left at 37°C for 24 h and then floated onto water, and the film obtained was laid onto acetone-cleaned nickel grids. The grids were placed on filter paper and left to dry for 12 h at room temperature before analysis by EM.

Lysozyme

Human wild-type lysozyme, expressed and purified from *Aspergillus niger* as described previously (Spencer et al., 1999), was prepared by Andrew Spencer (Institute of Food Research, Norwich, UK). Fibrils were generated

by dissolving the protein to 10 mg/ml in 10 mM glycine buffer, pH 2, and incubating for 2 weeks or more at 57°C (Morozova-Roche et al., 2000). Fibril formation was assessed by EM.

Atomic force microscopy

Ambient imaging

For ambient imaging, fibril samples (0.5–50 μg/ml) were deposited on freshly cleaved mica (Agar Scientific, Cambridge, UK) and dried overnight at room temperature. Experiments were carried out with a MultiMode microscope (Digital Instruments, Ltd., U.K.) in conjunction with a Nanoscope IIIa control system. Both "E" and "J" scanners were used, with lateral ranges of ~10 μm and ~125 μm, respectively. Etched silicon probes, attached to triangular cantilevers 100–200 μm in length (Digital Instruments, model TESP), were operated at resonances in the 300–400 kHz range (drive 400-1500 mV). Height, amplitude, and phase data were simultaneously collected, the latter with a Digital Instruments phase extender module. Before imaging, scanner calibration in the *xy* plane was checked through the use of a 1-μm calibration grid (LOT Oriel, Surry, U.K.) and in the *z* direction by imaging atomic steps on a cleaved highly orientated pyrolytic graphite surface. Solutions of suspended fibrils were gently agitated to ensure that selected aliquots were representative of the sample bulk. Samples were engaged at zero scan size to minimize possible contamination (biofouling) of the probe. Topographic data were regularly recorded simultaneously in trace and retrace to check for scan artifacts. Scan rates were 1–5 Hz.

Fluid phase imaging

Fluid phase imaging was carried out by depositing fibril solutions (0.5–50 μg/ml) on freshly cleaved mica and allowing the samples to stand for 10–30 min. The mica surface was then washed under a gentle stream of the buffer solution appropriate for imaging (see below) and placed into the Digital Instruments fluid cell. The cell was used without the supplied O-ring. Imaging was generally carried out under deionized water (18.2 MΩ, USF Elga, Buckinghamshire, U.K.), although to exclude the possibility of nonspecific electrostatic effects between the sample and the tip, lysozyme fibrils were also imaged under 15 and 100 mM potassium phosphate buffer, pH 7.4. Silicon nitride cantilevers (NP-STT), force constant 0.48 N/m (Digital Instruments) were used at a resonant frequency of 7–9 kHz. Data sets were subjected to a first-order flattening and low band pass filtering only where stated. Thermal noise levels are estimated to be ~ 0.1 nm. Fibril heights are estimated to be accurate to ±0.4 nm on the basis of the cross-sectional baseline errors.

RESULTS

TTR_{10-19} fibrils

Recent studies of amyloid fibrils by AFM are almost equally divided between those performed on fibril samples dried on a surface (Roher et al., 1996; Ionescu-Zanetti et al., 1999; Kayed et al., 1999; Blackley et al., 1999; Harper et al., 1999) and those performed under solvent (Müller et al., 1997; Goldsbury et al., 1999; Kowalewski and Holtzman, 1999; Lin et al., 1999). Fig. 1 compares fibrils assembled from TTR_{10-19} and observed by standard EM techniques (Fig. 1 *A*) with AFM images of fibrils deposited on freshly cleaved mica and dried overnight at room temperature (Fig. 1 *B*) or deposited and imaged under water (Fig. 1 *C*). The visible structural features are qualitatively similar in each case, although the fibrils imaged by AFM are significantly broadened due to convolution effects arising from the finite width of the AFM tip. All fibril dimensions were therefore estimated from the height of the fibril in cross section. Interestingly, the diameters of the fibrils estimated from electron micrographs or from AFM images acquired in air are significantly (1–2 nm) larger than the fibril diameters estimated from AFM images acquired under fluid. The average diameter of TTR_{10-19} fibrils estimated from EM data is 6.2 nm, although we estimate the error associated with this measurement to be as high as 1.5 nm. This value agrees well with the diameter of air-dried TTR_{10-19} fibrils estimated from AFM data (5.6 nm ± 0.6 nm). In contrast,

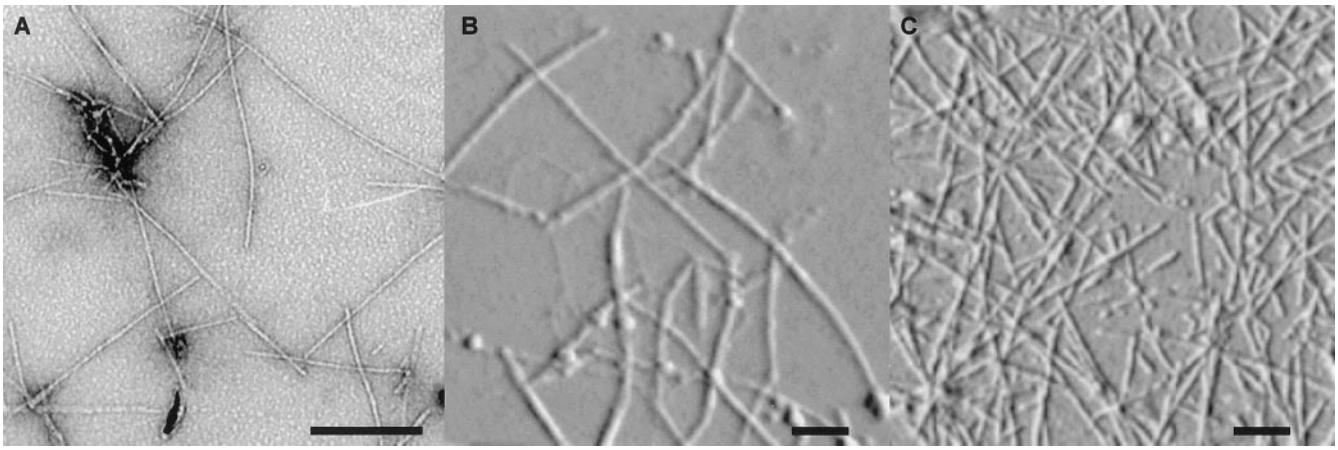

FIGURE 1 Images of fibrils assembled from TTR_{10-19}. (*A*) Transmission electron micrograph of uranyl acetate negatively stained fibrils. Scale bar, 200 nm. (*B*) Amplitude AFM image of TTR_{10-19} fibrils dried on the mica surface. Note that the fibril widths appear much larger in the AFM images than in electron micrographs due to convolution of surface features with the scanning tip. Scale bar, 200 nm. (*C*) Amplitude AFM image of TTR_{10-19} fibrils imaged in solution. The data have been subjected to a first-order flattening. Scale bar, 200 nm. Note that data within amplitude images represent an error signal. Although accentuating certain surface features, such images contain no true height information.

the average diameter of the fibrils imaged in solution by AFM is 4.4 nm (Fig. 2 *A*). A similar phenomenon has been noted by Goldsbury and coworkers (1999), who compared the dimensions of amylin fibrils imaged by EM with those grown in situ and monitored by AFM. Vertical measurements of biomolecules by AFM are free from the convolution effects associated with lateral measurements. They are, however, commonly inconsistent with crystallographic data, as a result of mechanical and electrostatic contributions to the imaging process. Goldsbury et al. ascribed their observations, in part, to electrostatic effects. In comparing data obtained in 100 mM potassium phosphate buffer with that in pure, deionized, water, we conclude that these effects are negligible. Instead, we ascribe the apparent discrepancy between the diameters of fibrils imaged in air and in solution primarily to the flexibility of hydrated biological specimens in response to the force applied by the oscillating AFM tip.

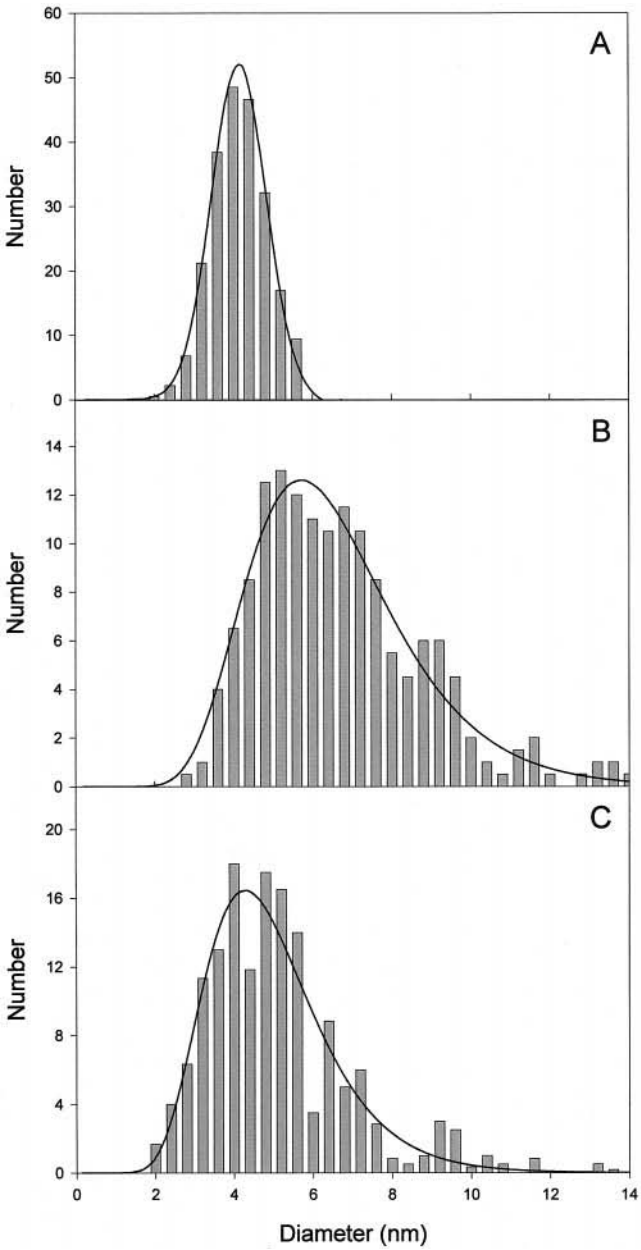

FIGURE 2 The dimensions of amyloid fibrils analyzed by AFM. (*A*) The diameter of TTR_{10-19} fibrils was assessed by measuring the height in cross section of >200 individual fibrils. The diameter of SH3 domain (*B*) and lysozyme (*C*) fibrils was assessed by measuring the height in cross section of ~150 individual fibrils. The broad distribution of diameters arises principally from structural heterogeneity within the fibrils. The data in each case have been fitted to a modified gaussian distribution for clarity (*solid lines*).

SH3 domain fibrils

EM and AFM images of SH3 domain fibrils are shown in Fig. 3, *A* and *B*, respectively. Once again, comparison of the AFM images with EM data indicates significant broadening of the apparent fibril width due to convolution with the AFM tip. The fundamental features of the fibrils are, nonetheless, similar. Unlike the TTR_{10-19} fibrils, which appear fairly uniform with respect to the fibril diameter, the structures assembled from the SH3 domain are highly heterogeneous and are made up of tubular fibrils, flat ribbons and twisted sheets. When the dimension of the fibrils are, once again, estimated from the height of the fibril in cross section, the heterogeneity in fibril structure gives rise to a very broad distribution of fibril diameters (Fig. 2 *B*). A different aspect of this variability is illustrated in Fig. 4 *A*, which shows a single SH3 domain fibril with a clearly visible left-handed twist that repeats along the fibril length. The handedness of this twist repeat was confirmed by EM of a fibril stained by unidirectional platinum shadowing as demonstrated in Fig. 4 *B*. The periodicity of this repeat is 104 ± 16 nm, and when viewed in cross section (Fig. 4 *C*) the fibril height oscillates between ~11 nm and ~6 nm. In such twisted structures the measured fibril height will clearly depend on the point at which it is measured along the fibril length.

The mean heights of individual fibrils were found to extend across a broad range of values. The fibril shown in Fig. 4 *A*, for example, has a height of 7.8 ± 0.6 nm, whereas others within the same sample ranged between 2 and 9 nm. Variations in the average fibril height have previously been ascribed to discrete populations of fibrils containing variable numbers of the protofilaments that make up the fibril substructure (Ionescu-Zanetti et al., 1999). On the basis of this assumption, and in the light of information derived from cryo-EM data (Jiménez et al., 1999), it is possible to tentatively assign the 7.8-nm fibrils as those containing four protofilaments, whereas fibrils with heights in the 4-nm range (Fig. 4 *C*) probably contain two protofilaments. An alternative explanation, however, is that the loosely twisted ribbon-like fibrils and the tightly twisted tubular fibrils are different forms of the same basic structure. Within this

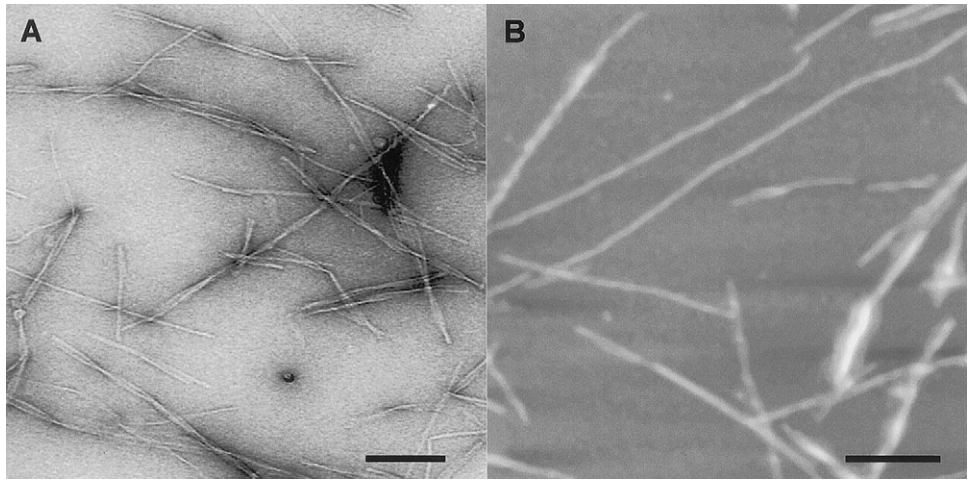

FIGURE 3 The structure of fibrils assembled from the SH3 domain of PI-3′-kinase. (*A*) Transmission electron micrograph of uranyl acetate negatively stained fibrils. Scale bar, 200 nm. (*B*) Height AFM image of SH3 domain fibrils imaged in solution. Scale bar, 200 nm; *z*-scale, 0–90 nm.

argument, then, the compactness of tubular fibrils is due to a change in the periodicity of the fibril twist. As with any elastic compound, a decrease in the twist repeat (a tighter twist) will give rise to an increase in the average diameter of the fibril. This hypothesis is supported by the observation that a fibril with an average diameter of 4.3 nm (Fig. 4 *C*) has an average repeat periodicity of 156 ± 16 nm and is thus less tightly twisted than the fibril with an average diameter of 7.8 nm. A low-diameter fibril with a long twist repeat is suggestive of a loosely coiled ribbon-like topog-

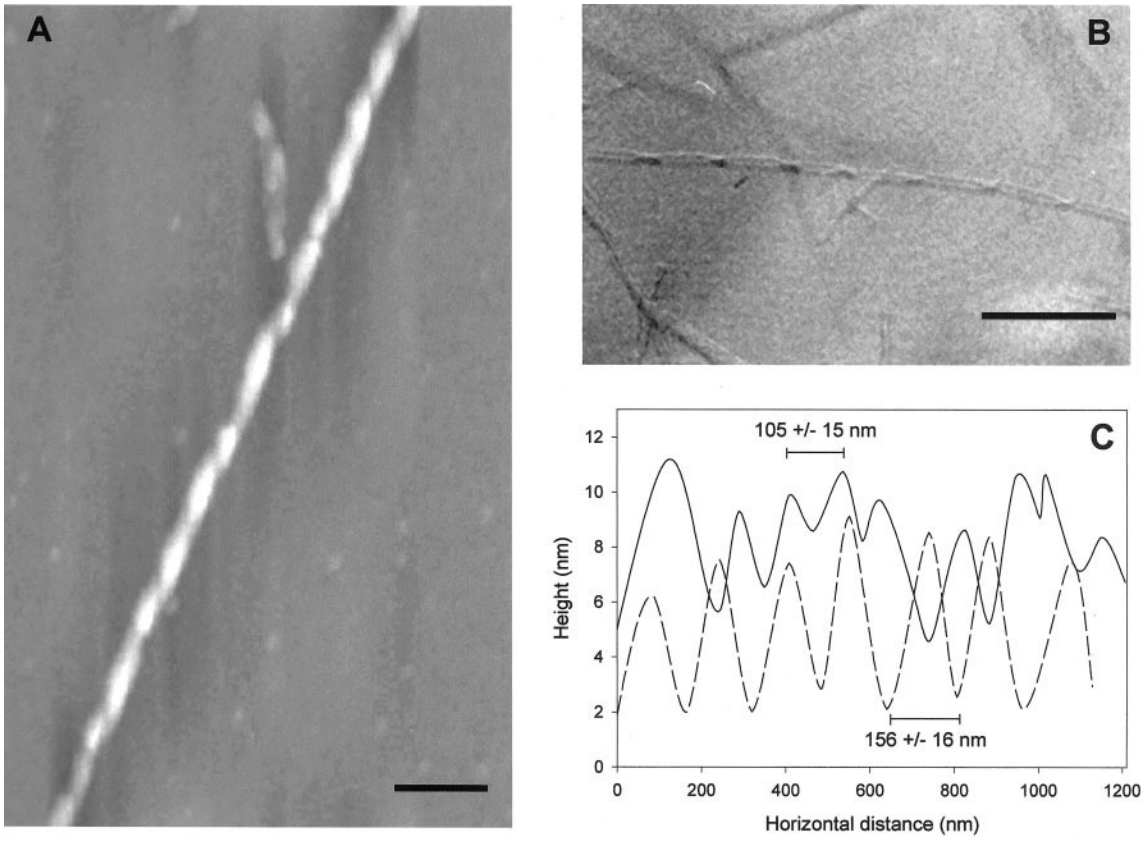

FIGURE 4 The fine structure of amyloid fibrils assembled from the SH3 domain of PI-3′-kinase. (*A*) Height AFM image of an SH3 domain fibril in solution. The twist repeat along the fibril axis is left-handed, with a periodicity of 104 ± 16 nm. Scale bar, 200 nm. (*B*) The handedness of the twist repeat is confirmed by electron microscopy of an SH3 domain fibril stained using unidirectional platinum shadowing. Scale bar, 200 nm. (*C*) Fibril height profiles along the axis of two fibrils with differing periodicities. The thinner fibril (average diameter, 4.3 nm; d*otted line*) has a longer axial repeat distance (156 ± 16 nm) than the larger fibril (average diameter, 7.8 nm; *solid line*).

raphy. A linear relationship between fibril diameter and helical repeat periodicity was applicable to the majority of SH3 domain fibrils examined.

A single ribbon-like SH3 domain fibril is shown in greater detail in Fig. 5. The fibril consists of clearly resolved substructures or protofilaments. A cross section taken through the fibril gives rise to the height profile shown in Fig. 5 *B*. We estimate the diameter of each protofilament to be approximately 2.3 nm by dividing the dimensions measured in cross section by a normalization factor (calculated with the simplifying assumption of a cylindrical cross section).

Human wild-type lysozyme fibrils

A similar arrangement of protofilaments to that of the SH3 domain fibrils is observed in fibrils assembled from the 130-residue protein lysozyme. Fig. 6 *A* shows fluid-phase imaging of a single lysozyme fibril that splays apart into four individual protofilaments. The lateral association of two protofilaments is shown in Fig. 6 *B*. The material observed in the background of both images is assumed to be small aggregates of the protein deposited on the mica surface. Protofilament diameters were measured from cross-sectional heights only in regions of the image where this amorphous material was not present. The lysozyme protofilaments have a diameter of 4.8–5.0 nm, more than twice the size of the SH3 domain protofilaments. These appear to coil together to form the numerous types of fibrils observed by EM and AFM; a typical selection is presented in Fig. 7. The fibril imaged by AFM and indicated by a solid arrow in Fig. 7 *B*, for example, consists of two substructures that coil in a left-handed manner to generate a loosely packed fibril with a regular axial crossover repeat interval of ~200 nm. Each substructure appears to consist of two coiled protofilaments, as each is too large (~8.3 nm diameter) to be a single protofilament. Thus, this loosely coiled fibril appears to be made up of four protofilaments arranged within a double helix. Also present in the AFM image presented in Fig. 7 *B* are several tubular fibrils, with axial crossover repeats exhibiting periodicities ranging from 80–160 nm. The diverse range of lysozyme fibril structures observed by AFM is therefore the reason for measured diameters, as with fibrils measured from the SH3 domain, crossing a broad distribution of values (Fig. 2 *C*).

DISCUSSION

AFM has been applied to the imaging of numerous fibrous systems of biological interest, including collagen and keratin (Gale et al., 1995; Paige et al., 1998; Parbhu et al., 1999), the paired helical filaments (PHFs) that make up a second pathological indicator of Alzheimer's disease (Pollanen et al., 1997), and amyloid fibrils (Roher et al., 1996; Conway et al., 1998; Wong et al., 1998; Harper et al., 1997a,b; 1999). Such is the power of fluid-phase imaging that it has enabled investigation of the superstructure of living cells (Henderson et al., 1992; Kasas et al., 1993) and the real-

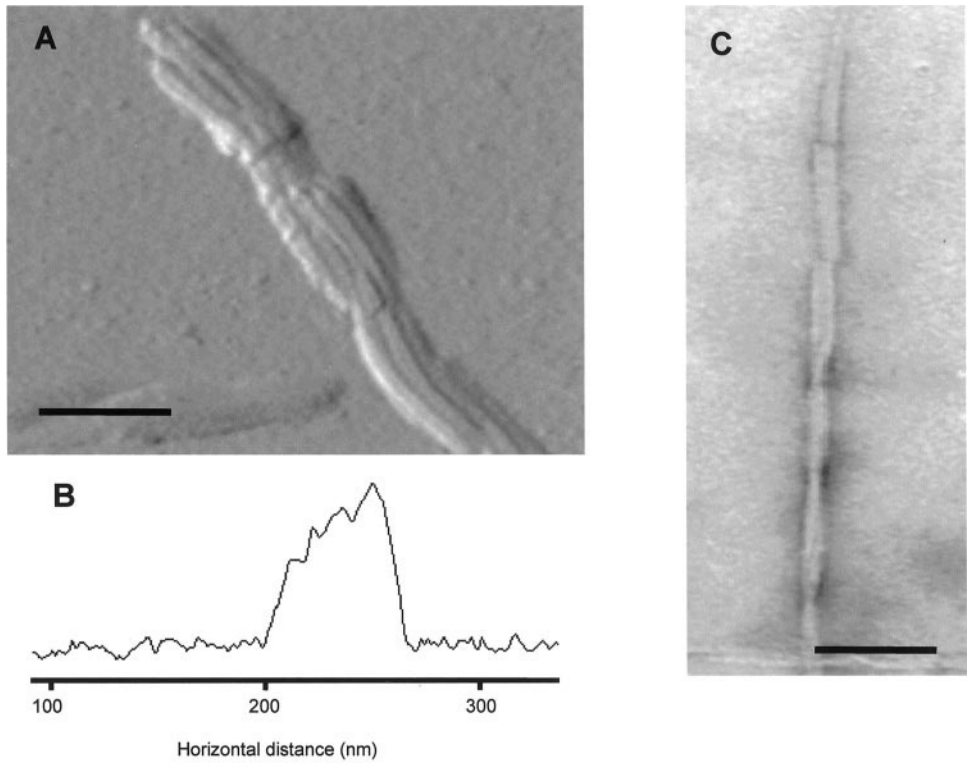

FIGURE 5 The fine structure of ribbon-like fibrils assembled from the SH3 domain. (*A*) Amplitude AFM image of a single amyloid fibril showing a loose twist of the ribbon-like structure containing four protofilaments. The image data have been low bandpass filtered to reduce noise and subjected to a first-order flattening. (*B*) Cross section profile for the fibril presented in *A*. (*C*) Transmission electron micrograph of a SH3 domain ribbon-like fibril. Scale bar, 100 nm.

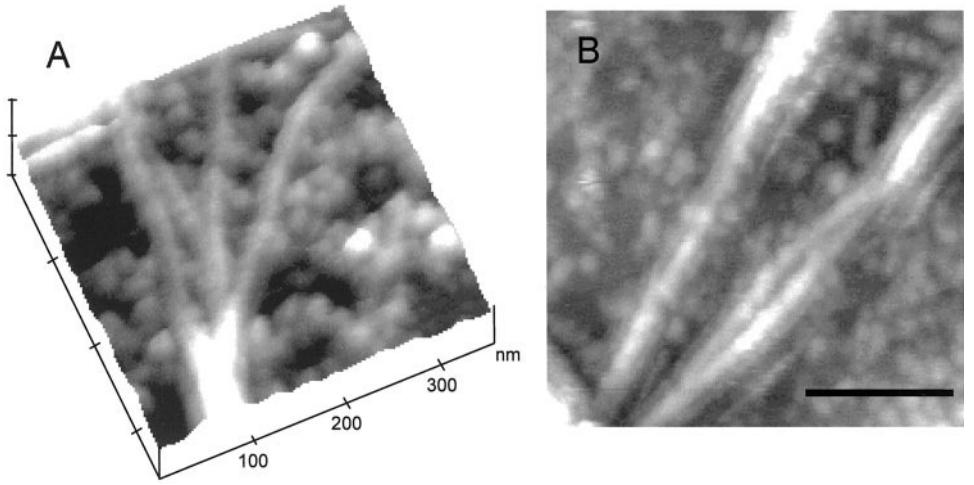

FIGURE 6 The fine structure of human wild-type lysozyme fibrils. (*A*) Three-dimensional AFM height image of a single lysozyme fibril that splays apart to form four distinct protofilaments. Each protofilament has an average diameter of close to 6.2 nm. *z*-scale, 0–30 nm. (*B*) A high-magnification amplitude AFM image showing the association of two protofilaments (each of 6–6.5 nm diameter). Scale bar, 200 nm; *z*-scale, 0–70 nm.

time growth of amyloid fibrils (Goldsbury et al., 1999). We have applied this technique to an investigation of the ultrastructural organization of three types of amyloid fibril that we prepare in the laboratory and have no known role in any human disease.

The ultrastructure of amyloid fibrils has been studied by numerous methods, including EM, x-ray diffraction, AFM, molecular modeling, and solid-state NMR. Data describing amyloid fibrils formed from a variety of protein precursors are summarized in Table 1. Most of the fibril systems that have been studied in detail previously were first recognized for their importance in human diseases, and, other than the SH3 domain and acylphosphatase, all of the proteins listed in Table 1 are related to disease processes. Some general trends appear to be common to fibrils formed by all proteins. The basic structural units, the protofilaments, are of the order of 2–5 nm in diameter and appear to be composed of between two and six β-sheets, depending on the protein system under investigation. The size of the protofilament is dictated by the association of β-sheets but is not related to the number of amino acid residues of the protein precursor. Thus, an 11-residue peptide derived from apo-SAA appears to form the largest protofilaments, comprising a putative six β-sheets, whereas the 90-residue SH3 domain forms protofilaments approximately 2 nm in diameter and apparently consisting of only two β-sheets. We predict from the dimensions of the human wild-type lysozyme protofilament measured by AFM (4.8–5.0 nm) that this 130-residue protein forms protofilaments comprising four β-sheets, similar to the protofilaments formed by transthyretin. The consis-

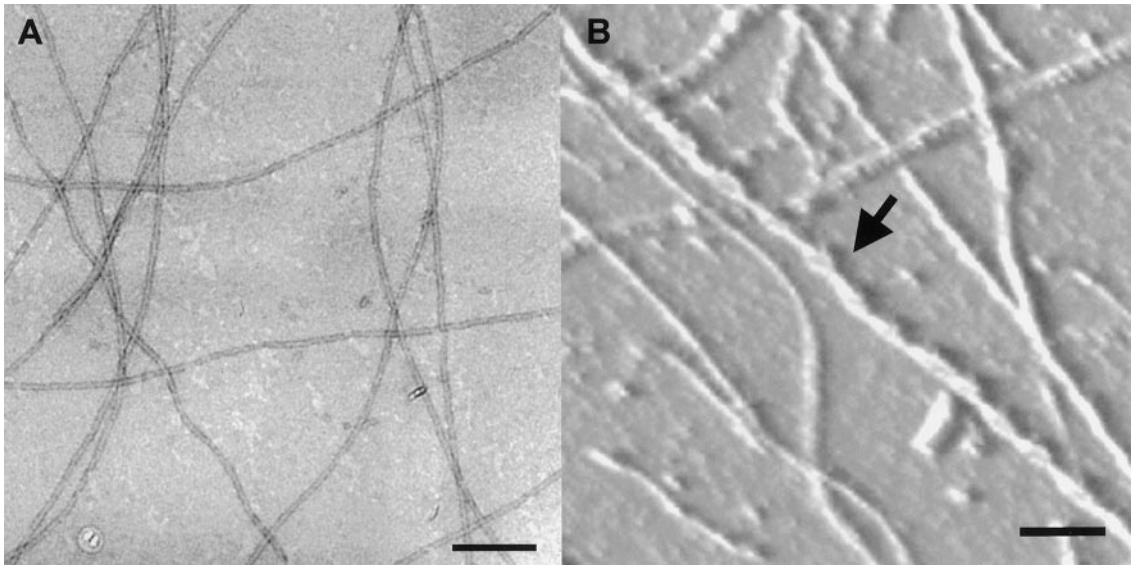

FIGURE 7 The structure of fibrils assembled from human lysozyme. (*A*) Transmission electron micrograph of uranyl acetate negatively stained fibrils. Scale bar, 200 nm. (*B*) Amplitude AFM image of lysozyme fibrils in solution. Scale bar, 400 nm.

TABLE 1 Amyloid fibril data

Fibril subunit	Number of residues	Diameter of protofilament (Å)	Number of sheets/ protofilament	Diameter of fibril (Å)	Number of protofilaments/fibril	Reference
Aβ(14–23)	10	40	2	N/A	N/A	Tjernberg et al., 1999
Aβ(6–25)	20	25–30	2	50–80	5–6	Fraser et al., 1991
Aβ(12–42)	31	40	4	N/A	N/A	Li et al., 1999
Aβ(1–40)	40	30–40	N/A	~90	2	Harper et al., 1997a, b
Aβ(1–40)	40	30	2	60–70	3–5	Malinchik et al., 1998
Aβ(1–42)	42	25–30	2	60–120	3–6	Chaney et al., 1998
ApoSAA	11	50–60	4–6	N/A	N/A	Kirschner et al., 1998
Calcitonin	32	40	N/A	80	3	Bauer et al., 1995
Amylin (IAPP)	37	24–50	N/A	80–130	2–4	Goldsbury et al., 1997; 1999
PrP^{Sc} (90–145)	56	40	2	80–100	4	Inouye and Kirschner, 1997
SH3 domain	90	20	2	100–130	4	Jiménez et al., 1999
Acylphosphatase	98	30–50	N/A	800–1500	>100	Chiti et al., 1999
Ig light chain	108?	24	N/A	60–91	4–6	Ionescu-Zanetti et al., 1999
Transthyretin	127	40–50	4	130	4	Serpell et al., 1995
Transthyretin	127	20	2	80–120	4	Inouye et al., 1998
PrP^{res}	>200	30–50	N/A	70–90	2	Merz et al., 1983

tency of the data within Table 1 and the similarity of our data to amyloid fibrils related to human disease support a general mechanism for amyloid assembly.

No information at present can be obtained on the substructure of fibrils assembled from TTR_{10-19}, because the AFM data indicate that they are remarkably uniform with respect to diameter. There is no evidence of the periodicity typical of both the SH3 domain and lysozyme fibrils. TTR_{10-19} protofilaments have, however, been observed previously in the presence of low concentrations of denaturant that appears to perturb inter-protofilament interactions (MacPhee and Dobson, 2000). These results suggest that the protofilament packing that drives the assembly of fibrils of TTR_{10-19} is relatively uniform, given the narrow distribution of fibril dimensions, and gives rise to a highly stable structure.

The fibril preparations described in the current work were all incubated for at least 2 weeks before examination by AFM and hence consist primarily of mature fibrils. We have chosen to refer to the relatively straight and long (>500-nm) fibril substructures observed by AFM and EM as protofilaments. Harper et al., (1997a,b) use the term protofilament to refer to the short and flexible structures present in immature fibril samples, and to the relatively long and straight substructures within mature fibrils as filaments or filamentous subunits. In contrast, Goldsbury et al. (1997, 1999) refer to the smallest unit structures of mature fibrils as protofilaments, described as having long, relatively rigid substructures. This definition derives from early observations dating back to the pioneering work of Cohen and others (see Cohen et al., 1982, for review) describing the ultrastructure of amyloid fibrils by electron microscopy of thin tissue sections. The distinction between these two definitions is, at least in part, a temporal one, as Harper and coworkers use the term protofilament to describe a structure that later assembles into mature fibrils.

It is useful to compare the conclusions of a cryo-EM study of SH3 domain fibrils (Jiménez et al*.,* 1999) with the AFM data presented here. The estimated size of the protofilaments observed within twisted ribbons by AFM (2.3 nm) agrees remarkably well with the model of a twisted fibril generated from cryo-EM data (~2 nm), and the observation of four protofilaments by AFM is, again, consistent with this. Both EM and AFM also show the formation of fibrils with differing morphology, the diversity apparently arising from the organization of the protofilaments within the fibril. The cryo-EM fibril model consists of four protofilaments super-coiled as a double helix along the length of the fiber axis. In other fibrils, observed both by AFM and in cryo-EM samples, the four protofilaments appear to be twisted as a single unit around the axis of the fiber, giving rise to a ribbon-like structure rather than a tubular fibril. It is unclear whether the ribbon-like structures are closely related to the tubular fibrils or whether these two types of fibril represent distinct arrangements of the protofilaments. Analysis of our AFM data suggests, however, that at least a proportion of fibrils differ only in the tightness of the helical pitch of the four laterally associated protofilaments along the long axis of the fibril (Fig. 4 *C*). It is possible, therefore, that the tubular fibrils merely represent the tightest possible twist of the protofilament ribbon about the fibril axis.

The protofilaments within the assembled fibril of the SH3 domain could be four independent units or two pairs of protofilaments where the β-sheets within each are joined by a stretch of unstructured polypeptide chain. Cryo-EM diffraction data indicate an apparent twofold axis of symmetry in the electron density, which is perhaps suggestive of a covalent linkage between the two protofilaments (Jiménez et al., 1999). Neither structural arrangement can, however, be unequivocally confirmed by the AFM data. Although four substructures can be observed (Fig. 5) in many of the SH3 domain fibrils examined by AFM, splitting of the

fibrils into independent substructures, as seen for human wild-type lysozyme, was not detected in the analyzed samples. A substructure composed of two covalently linked protofilaments could still give rise to both the twisted ribbons and compact tubular fibrils observed in SH3 domain fibril preparations.

Formation of mature fibrils by protofilament self-association appears to be influenced by the nature of the constituent protein species. Fibrils assembled from an immunoglobulin light chain have been classified into two classes: type I and type II fibrils consisting of six or four protofilaments, respectively (Ionescu-Zanetti et al., 1999). Islet amyloid polypeptide (amylin), the amyloidogenic protein precursor implicated in type-II diabetes, displays further polymorphism, forming discrete ribbons consisting of two, three, or four laterally associated protofilaments, tubular fibrils, and occasionally flat sheets (Goldsbury et al., 1997). Importantly, fibril morphology is also sensitive to the conditions under which the fibrils are formed. Human calcitonin fibrils assembled in vitro display significant morphological polymorphism that correlates with the history and concentration of solutions of the protein precursor (Bauer et al., 1995). A large body of evidence is available suggesting that the morphology and biological behavior (Busciglio et al., 1992; Seilheimer et al., 1997) of the Aβ peptide implicated in Alzheimer's disease is related both to solvent exposure before amyloid assembly and to the exact conditions employed for fibril growth (Shen et al., 1994; Soto and Frangione, 1995; Shen and Murphy, 1995).

The question therefore arises as to how the specific protein sequence and the local environment affect the association of the protofilaments and give rise to a heterogeneous population of fibrillar structures. The ready formation of amyloid by a 10-residue peptide derived from the sequence of the Alzheimer's-related protein Aβ (Tjernberg et al., 1999) or a nine-residue peptide derived from the sequence of gelsolin (Maury et al., 1994) suggests that the cooperative association of only short regions of a protein is sufficient to generate a remarkably stable fibril structure. The importance of the protein main chain in the structure of amyloid, especially the β-sheet core of the protofilaments, provides an explanation for the formation of amyloid fibrils with a common structure by a wide variety of structurally unrelated proteins. It is likely, therefore, that the morphological diversity of the fibrils subsequently formed from the protofilaments arises from heterogeneous packing of those regions of the polypeptide chain that do not contribute to the β-sheet backbone but make up the interface between the protofilaments. These regions of polypeptide chain are likely to be disordered relative to the β-sheet structure of the amyloid fibrils. The presence of disordered material is evident from the electron-sparse regions of cryo-EM data acquired for SH3 domain fibrils and is thought to be composed of regions of the polypeptide chain that join adjacent β-strands within the protofilaments (Jiménez et al., 1999). Amorphous regions of polypeptide have also been inferred from x-ray diffraction studies of ex vivo and in vitro assembled fibrils (Sunde et al., 1997; Inouye et al., 1998). It should be noted, however, that so far there is no clear evidence by other techniques (Fourier transform infrared or circular dichroism) for the formation of a significant fraction of the polypeptide chain in a random coil structure within any type of amyloid fibril, suggesting that some degree of secondary and tertiary structure exists in these regions or that only a small proportion of the polypeptide chain contributes to the inter-strand linkages.

Heterogeneity in the organization of the disordered regions of the polypeptide chains would also provide a ready explanation for the formation, by the SH3 domain, of amyloid ribbons that appear to be twisted to various degrees. If such structures observed by AFM consist of four laterally associated protofilaments making up a ribbon-like structure that then twists to form progressively tighter tubular fibrils, then the inter-protofilament interactions must be relatively non specific to allow the protofilaments to reorganize relative to one another. The existence of disordered, amorphous regions of the polypeptide chain would permit some degree of flexibility in these interacting regions as the polypeptide chain could be rearranged to form the optimal packing of side chains at the interface and at the fibril surface. This model of fibril assembly also accounts for the ability of fibrils to mature and structurally rearrange with time (Seilheimer et al., 1997).

In all of the fibrils formed by the SH3 domain or human lysozyme observed within this AFM study that display a resolved twist repeat along the length of the fiber axis, the handedness of the twist is always to the left. Indeed, in the majority of cases where twisted fibril ultrastructures have been reported, a left-handed coiling about the fiber axis has been observed (Bauer et al., 1995; Goldsbury et al., 1997; Harper et al., 1997a; Ionescu-Zanetti et al., 1999). A notable exception to this are fibrils formed from peptides containing all D-amino acids (Harper et al., 1997a). These exhibit a right-handed coiling of the protofilaments, indicating that the twisting of protofilaments along the fibril axis is dictated by the chirality of the amino acids in the constituent protein species.

An important question is whether amyloid fibrils purified from tissue samples or prepared in vitro from disease-associated polypeptides actually represent the structures formed in vivo and implicated in the disease state itself. High-resolution ultrastructural investigations of thin-layer tissue sections by EM (Inoue and Kisilevsky, 1996; Inoue et al., 1997, 1998a,b) suggest that in vivo amyloid deposits consist of a core of amyloid P (AP) component and proteoglycans, surrounded by a loose network of heparan sulfate proteoglycans and thin filaments ($\sim$1 nm) of amyloidotic protein. Inoue et al. (1998a,b) suggest that only on extraction of the amyloid material do the thin protein filaments associate to form the structure typically thought of as amy-

loid. It is therefore important to examine a wide range of fibrillar structures in vitro and to investigate the binding of secondary components such as AP and proteoglycans to the fibrils. Integral to increasing our understanding of the structure and heterogeneity of amyloid samples, and the possible relevance of this to the clinical heterogeneity of associated disease states, will be the development of methods by which the properties of individual fibrillar structures can be probed. The ability to examine fibrils under solution by AFM provides an opportunity to study interactions of these with other molecules and to follow both the kinetics and mechanisms of fibril growth and dissolution at a nanometer resolution. Such investigations will provide a powerful means of scrutinizing the process of fibrillogenesis with renewed clarity as well as providing important information about the specific behavior of polypeptides implicated in the disease process in vivo.

We thank Maureen Pitkeathly for the synthesis and purification of TTR_{10-19}, Denis Canet for providing samples of human lysozyme, Emma Jaikaran for assistance with metal shadowing, and Mario Bouchard and Mark Krebs for valuable discussions and comments. The Oxford Centre for Molecular Sciences is supported by the U.K. Biotechnology and Biological Sciences Research Council, the Engineering and Physical Sciences Council, and the Medical Research Council. A.K.C. acknowledges support from the Helen Hay Whitney Foundation. L.A.M-R and J.Z. acknowledge support from the Wellcome Trust. C.E.M is a Royal Society Dorothy Hodgkin Research Fellow. The research of C.M.D. is supported in part by the Howard Hughes Medical Research Institute and by the Wellcome Trust. The research of H.A.O.H is supported by Abbott Diagnostics and Medisense Inc. J.J.D is a Royal Society University Research Fellow.

REFERENCES

Bauer, H. H., U. Aebi, M. Haner, R. Hermann, M. Muller, and H. P. Merkle. 1995. Architecture and polymorphism of fibrillar supramolecular assemblies produced by in vitro aggregation of human calcitonin. *J. Struct. Biol.* 115:1–15.

Benzinger, T. L., D. M. Gregory, T. S. Burkoth, H. Miller-Auer, D. G. Lynn, R. E. Botto, and S. C. Meredith. 1998. Propagating structure of Alzheimer's β-amyloid(10–35) is parallel β-sheet with residues in exact register. *Proc. Natl. Acad. Sci. U.S.A.* 95:13407–13412.

Blackley, H. K., N. Patel, M. C. Davies, C. J. Roberts, S. J. Tendler, M. J. Wilkinson, and P. M. Williams. 1999. Morphological development of β(1–40) amyloid fibrils. *Exp. Neurol.* 158:437–443.

Blake, C., and L. Serpell. 1996. Synchrotron x-ray studies suggest that the core of the transthyretin amyloid fibril is a continuous β-sheet helix. *Structure.* 4:989–998.

Blake, C. C., L. C. Serpell, M. Sunde, O. Sandgren, and E. Lundgren. 1996. A molecular model of the amyloid fibril. *Ciba Found. Symp.* 199:6–15.

Booker, G. W., I. Gout, A. K. Downing, P. C. Driscoll, J. Boyd, M. D. Waterfield, and I. D. Campbell. 1993. Solution structure and ligand-binding site of the SH3 domain of the p85 α subunit of phosphatidylinositol 3′-kinase. *Cell.* 73:813–822.

Booth, D. R., M. Sunde, V. Bellotti, C. V. Robinson, W. L. Hutchinson, P. E. Fraser, P. N. Hawkins, C. M. Dobson, S. E. Radford, C. F. Blake, and M. B. Pepys. 1997. Instability, unfolding and aggregation of human lysozyme variants underlying amyloid fibrillogenesis. *Nature.* 385: 787–793.

Busciglio, J., A. Lorenzo, and B. A. Yankner. 1992. Methodological variables in the assessment of beta amyloid neurotoxicity. *Neurobiol. Aging.* 13:609–612.

Canet, D., M. Sunde, A. M. Last, A. Miranker, A. Spencer, C. V. Robinson, and C. M. Dobson. 1999. Mechanistic studies of the folding of human lysozyme and the origin of amyloidogenic behavior in its disease-related variants. *Biochemistry.* 38:6419–6427.

Chaney, M. O., S. D. Webster, Y. M. Kuo, and A. E. Roher. 1998. Molecular modeling of the Aβ1–42 peptide from Alzheimer's disease. *Protein Eng.* 11:761–767.

Chiti, F., P. Webster, N. Taddei, A. Clark, M. Stefani, G. Ramponi, and C. M. Dobson. 1999. Designing conditions for in vitro formation of amyloid protofilaments and fibrils. *Proc. Natl. Acad. Sci. U.S.A.* 96: 3590–3594.

Cohen, A. S., T. Shirahama, and M. Skinner. 1982. Electron microscopy of amyloid. *In* Electron Microscopy of Proteins. J. R. Harris, editor. Academic Press, New York. 165–205.

Conway, K. A., J. D. Harper, and P. T. Lansbury. 1998. Accelerated in vitro fibril formation by a mutant α-synuclein linked to early-onset Parkinson disease. *Nature Med.* 4:1318–2130.

Dobson, C. M. 1999. Protein misfolding, evolution and disease. *Trends Biochem. Sci.* 24:329–332.

Engel, A., H. E. Gaub, and D. J. Muller. 1999. Atomic force microscopy: a forceful way with single molecules. *Curr. Biol.* 9:R133–R-136.

Fraser, P. E., L. K. Duffy, M. B. O'Malley, J. Nguyen, H. Inouye, and D. A. Kirschner. 1991. Morphology and antibody recognition of synthetic β-amyloid peptides. *J. Neurosci. Res.* 28:474–485.

Gale, M., M. S. Pollanen, P. Markiewicz, and M. C. Goh. 1995. Sequential assembly of collagen revealed by atomic force microscopy. *Biophys. J.* 68:2124–2128.

Goldsbury, C. S., G. J. Cooper, K. N. Goldie, S. A. Muller, E. L. Saafi, W. T. Gruijters, M. P. Misur, A. Engel, U. Aebi, and J. Kistler. 1997. Polymorphic fibrillar assembly of human amylin. *J. Struct. Biol.* 119: 17–27.

Goldsbury, C., J. Kistler, U. Aebi, T. Arvinte, and G. J. S. Cooper. 1999. Watching amyloid fibrils grow by time-lapse atomic force microscopy. *J. Mol. Biol.* 285:33–39.

Guijarro, J. I., C. J. Morton, K. W. Plaxco, I. D. Campbell, and C. M. Dobson. 1998a. Folding kinetics of the SH3 domain of PI3′-kinase by real-time NMR combined with optical spectroscopy. *J. Mol. Biol.* 276: 657–667.

Guijarro, J. I., M. Sunde, J. A. Jones, I. D. Campbell, and C. M. Dobson. 1998b. Amyloid fibril formation by an SH3 domain. *Proc. Natl. Acad. Sci. U.S.A.* 95:4224–4228.

Gustavsson, A., U. Engstrom, and P. Westermark. 1991. Normal transthyretin and synthetic transthyretin fragments form amyloid-like fibrils in vitro. *Biochem. Biophys. Res. Commun.* 175:1159–1164.

Hansma, H. G., and J. H. Hoh. 1994. Biomolecular imaging with the atomic force microscope. *Annu. Rev. Biophys. Biomol. Struct.* 23: 115–139.

Harper, J. D., C. M. Lieber, and P. T. Lansbury. 1997a. Atomic force microscopic imaging of seeded fibril formation and fibril branching by the Alzheimer's disease amyloid-β protein. *Chem. Biol.* 4:951–959.

Harper, J. D., S. S. Wong, C. M. Lieber, and P. T. Lansbury. 1997b. Observation of metastable Aβ amyloid protofibrils by atomic force microscopy. *Chem. Biol.* 4:119–125.

Harper, J. D., S. S. Wong, C. M. Lieber, and P. T. Lansbury. 1999. Assembly of Aβ amyloid protofibrils: an in vitro model for a possible early event in Alzheimer's disease. *Biochemistry.* 38:8972–8980.

Heinz, W. F., and J. H. Hoh. 1999. Spatially resolved force spectroscopy of biological surfaces using the atomic force microscope. *Trends Biotechnol.* 17:143–150.

Henderson, E., P. G. Haydon, and D. S. Sakaguchi. 1992. Actin filament dynamics in living glial cells imaged by atomic force microscopy. *Science.* 257:1944–1946.

Inoue, S., and R. Kisilevsky. 1996. A high resolution ultrastructural study of experimental murine AA amyloid. *Lab. Invest.* 74:670–683.

Inoue, S., M. Kuroiwa, K. Ohashi, M. Hara, and R. Kisilevsky. 1997. Ultrastructural organization of hemodialysis-associated β2-microglobulin amyloid fibrils. *Kidney Int.* 52:1543–1549.

Inoue, S., M. Kuroiwa, M. J. Saraiva, A. Guimaraes, and R. Kisilevsky. 1998a. Ultrastructure of familial amyloid polyneuropathy amyloid fibrils: examination with high-resolution electron microscopy. *J. Struct. Biol.* 124:1–12.

Inoue, S., M. Kuroiwa, R. Tan, and R. Kisilevsky. 1998b. A high resolution ultrastructural comparison of isolated and in situ murine AA amyloid fibrils. *Amyloid.* 5:99–110.

Inouye, H., F. S. Domingues, A. M. Damas, M. J. Saraiva, E. Lundgren, O. Sandgren, and D. A. Kirschner. 1998. Analysis of x-ray diffraction patterns from amyloid of biopsied vitreous humor and kidney of transthyretin (TTR) Met30 familial amyloidotic polyneuropathy (FAP) patients: axially arrayed TTR monomers constitute the protofilament. *Amyloid.* 5:163–174.

Inouye, H., and D. A. Kirschner. 1997. X-ray diffraction analysis of scrapie prion: intermediate and folded structures in a peptide containing two putative α-helices. *J. Mol. Biol.* 268:375–389.

Ionescu-Zanetti, C., R. Khurana, J. R. Gillespie, J. S. Petrick, L. C. Trabachino, L. J. Minert, S. A. Carter, and A. L. Fink. 1999. Monitoring the assembly of Ig light-chain amyloid fibrils by atomic force microscopy. *Proc. Natl. Acad. Sci. U.S.A.* 96:13175–13179.

Jarvis, J. A., D. J. Craik, and M. C. Wilce. 1993. X-ray diffraction studies of fibrils formed from peptide fragments of transthyretin. *Biochem. Biophys. Res. Commun.* 192:991–998.

Jiménez, J. L., J. I. Guijarro, E. Orlova, J. Zurdo, C. M. Dobson, M. Sunde, and H. R. Saibil. 1999. Cryo-electron microscopy structure of an SH3 amyloid fibril and model of the molecular packing. *EMBO J.* 18: 815–821.

Kasas, S., V. Gotzos, and M. R. Celio. 1993. Observation of living cells using the atomic force microscope. *Biophys. J.* 64:539–544.

Kayed, R., J. Bernhagen, N. Greenfield, K. Sweimeh, H. Brunner, W. Voelter, and A. Kapurniotu. 1999. Conformational transitions of islet amyloid polypeptide (IAPP) in amyloid formation in vitro. *J. Mol. Biol.* 287:781–796.

Kelly, J. W. 1998. The alternative conformations of amyloidogenic proteins and their multi-step assembly pathways. *Curr. Opin. Struct. Biol.* 8:101–106.

Kirschner, D. A., R. Elliott-Bryant, K. E. Szumowski, W. A. Gonnerman, M. S. Kindy, J. D. Sipe, and E. S. Cathcart. 1998. In vitro amyloid fibril formation by synthetic peptides corresponding to the amino terminus of apoSAA isoforms from amyloid-susceptible and amyloid-resistant mice. *J. Struct. Biol.* 124:88–98.

Koo, E. H., P. T. Lansbury, and J. W. Kelly. 1999. Amyloid diseases: abnormal protein aggregation in neurodegeneration. *Proc. Natl. Acad. Sci. U.S.A.* 96:9989–9990.

Kowalewski, T., and D. M. Holtzman. 1999. In situ atomic force microscopy study of Alzheimer's β-amyloid peptide on different substrates: new insights into mechanism of β-sheet formation. *Proc. Natl. Acad. Sci. U.S.A.* 96:3688–3693.

Lansbury, P. T. 1999. Evolution of amyloid: what normal protein folding may tell us about fibrillogenesis and disease. *Proc. Natl. Acad. Sci. U.S.A.* 96:3342–3344.

Lansbury, P. T., P. R. Costa, J. M. Griffiths, E. J. Simon, M. Auger, K. J. Halverson, D. A. Kocisko, Z. S. Hendsch, T. T. Ashburn, and R. G. Spencer. 1995. Structural model for the β-amyloid fibril based on interstrand alignment of an antiparallel-sheet comprising a C-terminal peptide. *Nat. Struct. Biol.* 2:990–998.

Li, L., T. A. Darden, L. Bartolotti, D. Kominos, and L. G. Pedersen. 1999. An atomic model for the pleated β-sheet structure of Aβ amyloid protofilaments. *Biophys. J.* 76:2871–2878.

Lin, H., Y. J. Zhu, and R. Lal. 1999. Amyloid beta protein (1–40) forms calcium-permeable, Zn^{2+}-sensitive channel in reconstituted lipid vesicles. *Biochemistry.* 38:11189–11196.

MacPhee, C. E., and C. M. Dobson. 2000. Chemical dissection and reassembly of amyloid fibrils formed by a peptide fragment of transthyretin. *J. Mol. Biol.* 297:1203–1215.

Malinchik, S. B., H. Inouye, K. E. Szumowski, and D. A. Kirschner. 1998. Structural analysis of Alzheimer's β(1–40) amyloid: protofilament assembly of tubular fibrils. *Biophys. J.* 74:537–545.

Maury, C. P., E. L. Nurmiaho-Lassila, and H. Rossi. 1994. Amyloid fibril formation in gelsolin-derived amyloidosis: definition of the amyloidogenic region and evidence of accelerated amyloid formation of mutant Asn-187 and Tyr-187 gelsolin peptides. *Lab. Invest.* 70:558–564.

Merz, P. A., H. M. Wisniewski, R. A. Somerville, S. A. Bobin, C. L. Masters, and K. Iqbal. 1983. Ultrastructural morphology of amyloid fibrils from neuritic and amyloid plaques. *Acta Neuropathol.* 60: 113–124.

Morozova-Roche, L. A., J. Zurdo, A. Spencer, W. Noppe, V. Receveur, D. Archer, M. Joniau, and C. M. Dobson. 2000. Amyloid fibril formation and seeding by wild type human lysozyme and its disease related mutational variants, *J. Struct. Biol.* 130:339–351.

Müller, D. J., M. Amrein, and A. Engel. 1997. Adsorption of biological molecules to a solid support for scanning probe microscopy. *J. Struct. Biol.* 119:172–188.

Paige, M. F., J. K. Rainey, and M. C. Goh.1998. Fibrous long spacing collagen ultrastructure elucidated by atomic force microscopy. *Biophys. J.* 74:3211–3216.

Parbhu, A. N., W. G. Bryson, and R. Lal. 1999. Disulfide bonds in the outer layer of keratin fibers confer higher mechanical rigidity: correlative nano-indentation and elasticity measurement with an AFM. *Biochemistry.* 38:11755–11761.

Pepys, M. B., P. N. Hawkins, D. R. Booth, D. M. Vigushin, G. A. Tennent, A. K. Soutar, N. Totty, O. Nguyen, and C. C. F. Blake. 1993. Human lysozyme gene mutations cause hereditary systemic amyloidosis. *Nature.* 362:553–557.

Perutz, M. F. 1999. Glutamine repeats and neurodegenerative diseases: molecular aspects. *Trends Biochem. Sci.* 24:58–63.

Pollanen, M. S., P. Markiewicz, and M. C. Goh. 1997. Paired helical filaments are twisted ribbons composed of two parallel and aligned components: image reconstruction and modeling of filament structure using atomic force microscopy. *J. Neuropathol. Exp. Neurol.* 56:79–85.

Roher, A. E., M. O. Chaney, Y. M. Kuo, S. D.Webster, W. B. Stine, L. J. Haverkamp, A. S. Woods, R. J. Cotter, J. M. Tuohy, G. A. Krafft, B. S. Bonnell, and M. R. Emmerling. 1996. Morphology and toxicity of Aβ-(1–42) dimer derived from neuritic and vascular amyloid deposits of Alzheimer's disease. *J. Biol. Chem.* 271:20631–20635.

Seilheimer, B., B. Bohrmann, L. Bondolfi, F. Muller, D. Stuber, and H. Dobeli. 1997. The toxicity of the Alzheimer's β-amyloid peptide correlates with a distinct fiber morphology. *J. Struct. Biol.* 119:59–71.

Serpell, L. C., M. Sunde, and C. C. F. Blake. 1997. The molecular basis of amyloidosis. *Cell. Mol. Life Sci.* 53:871–887.

Serpell, L. C., M. Sunde, P. E. Fraser, P. K. Luther, E. P. Morris, O. Sangren, E. Lundgren, and C. C. F. Blake. 1995. Examination of the structure of the transthyretin amyloid fibril by image reconstruction from electron micrographs. *J. Mol. Biol.* 254:113–118.

Shao, Z., and J. Yang. 1995. Progress in high resolution atomic force microscopy in biology. *Q. Rev. Biophys.* 28:195–251.

Shao, Z., Yang, J., and A. P. Somlyo. 1995. Biological atomic force microscopy: from microns to nanometers and beyond. *Annu. Rev. Cell. Dev. Biol.* 11:241–265.

Shao, Z., and Y. Zhang. 1996. Biological cryo atomic force microscopy: a brief review. *Ultramicroscopy.* 66:141–152.

Shen, C. L., M. C. Fitzgerald, and R. M. Murphy. 1994. Effect of acid predissolution on fibril size and fibril flexibility of synthetic β-amyloid peptide. *Biophys. J.* 67:1238–12346.

Shen, C. L., and R. M. Murphy. 1995. Solvent effects on self-assembly of β-amyloid peptide. *Biophys. J.* 69:640–651.

Soto, C., and B. Frangione. 1995. Two conformational states of amyloid β-peptide: implications for the pathogenesis of Alzheimer's disease. *Neurosci. Lett.* 186:115–118.

Spencer, A., L. A. Morozov-Roche, W. Noppe, D. A. MacKenzie, D. J. Jeenes, M. Joniau, C. M. Dobson, and D. B. Archer. 1999. Expression, purification, and characterization of the recombinant calcium-binding equine lysozyme secreted by the filamentous fungus *Aspergillus niger*: comparisons with the production of hen and human lysozymes. *Prot. Exp. Purif.* 16:171–180.

Sunde, M., L. C. Serpell, M. Bartlam, P. E. Fraser, M. B. Pepys, and C. C. F. Blake. 1997. Common core structure of amyloid fibrils by synchrotron x-ray diffraction. *J. Mol. Biol.* 273:729–739.

Tjernberg, L. O., D. J. Callaway, A. Tjernberg, S. Hahne, C. Lilliehook, L. Terenius, J. Thyberg, and C. Nordstedt. 1999. A molecular model of Alzheimer amyloid β-peptide fibril formation. *J. Biol. Chem.* 274: 12619–12625.

Wong, S. S., J. D. Harper, P. T. Lansbury, and C. M. Lieber. 1998. Carbon nanotube tips: high-resolution probes for imaging biological systems. *J. Am. Chem. Soc.* 120:603–604.